View metadata, citation and similar papers at core.ac.uk

brought to you by CORE

provided by NASA Technical Reports Server

NAS III - 2671

DRA

Report No.950/1

EFFECT OF GRAVITY ON METHANE-AIR COMBUSTION

(NASA-CR-135077) EFFECT OF GRAVITY ON METHANE-AIR COMBUSTION (Combustion, Heat, and Mass Transfer Ltd.) 70 p HC $4.50 CSCL 21B

N76-29381

Unclas G3/25 48955

AUG 1976 RECEIVED NASA STI FACILITY INPUT BRANCH

ORIGINAL PAGE IS OF POOR QUALITY

APR 1975 RECEIVED NASA STI FACILITY INPUT BRANCH

Prepared for

NASA Lewis Research Center,

Cleveland, Ohio, U.S.A.

CHAM, Combustion, Heat and Mass Transfer Ltd.

86 Burlington Road, New Malden, Surrey,

England.

December 22, 1974.

FOREWORD

This technical report was prepared by CHAM, Combustion Heat and Mass Transfer, New Malden, Surrey, England, under Contract No.NASW - 2671 and CHAM Project No.950.

The computations were carried out by H.I. Rosten and A. K.Runchal.

The report was prepared by S. Elghobashi, H.I. Rosten, J. E.Smith, D.B. Spalding and D.G. Tatchell.

CONTENTS PAGE

1. INTRODUCTION

1.1. The Problem

The NASA Lewis Laboratory is conducting an investigation into the influence of zero and reduced gravitational acceleration on diffusion flames, with a view to improving understanding of fires in space vehicles. Experiments have been conducted by NASA Lewis personnel on the burning in air of a jet of methane emerging from a cylindrical tube; the air is at rest relative to the tube, apart from motion induced by the jet; the whole apparatus can be dropped down a tower, so that zero-gravity operation may be investigated.

In experiments in which the apparatus is first at rest, and then suddenly dropped, the flame length passes from one (nearly) steady value to another value, after passing through smaller transient values. The re-establishment of a steady state lasts about 0.5 seconds. The tube radius is in the range 0.05 to 0.44 cm, and the flow rate of methane is in the range 1 to 8 cm^3 per sec. The maximum velocity at the tube-exit axis is around 1200 cm per sec. The whole experiment lasts for about 5 seconds. The pressure is atmospheric, and the air- and gas- supply temperatures are around room temperature. The flow is laminar.

The NASA Lewis Laboratory wishes to compare its experimental findings with numerical solutions of the differential equations believed to govern the processes, with a view to confirming qualitative understanding of the process, to determine the quantitative accuracy of numerical predictions, and to establish a mathematical model of the process for subsequent use as a predictive and exploratory tool.

During recent years CHAM Ltd has developed a range of analytical models and numerical techniques to study fluid-dynamic, heat

discussion of the analytical results obtained in this study. The final chapter is devoted to concluding remarks concerning the computational accuracy, and efficiency of the computer code, together with an assessment of the physical realism of the results. In each case, suggestions are made concerning means by which they may be improved.

1.2. Previous Work

The earlier analytical study of steady laminar diffusion flames can be categorised in terms of firstly, semi-empirical approaches based upon correlations of specific data (see typically Refs 1 and 2) and secondly, special solutions of the conservation equations (e.g. Refs 3 and 4). These have been summarised in References 5 and 6. These approaches either ignored the effects of gravity or provided inadequate agreement with experiment when gravitional effects are significant.

More recent developments using more precise numerical techniques allied with greater computing power in modern computers have enabled more sophisticated analytical models to be studied. These developments recognise the need to solve the equations for mass, momentum and energy in circumstances which take into account interdependence of the velocity, temperature and concentration fields. These methods also use finite-difference forms of the governing differential equations which reduces the restrictions on the generality of the boundary conditions and provide a framework for rapid development of the analytical models to include for example the effects of gravity. Edelman et al.(Ref 7) developed a model with sufficient generality that further insights could be gained concerning the effects of gravity on steady laminar diffusion flames. Good agreement was achieved with experimental results in normal-g flames, however, predictions were not so good under conditions of zero gravity.

transfer and combustion problems. These models and techniques have been applied to a variety of problems, both steady and unsteady, with and without chemical reaction. The major purpose of the study described in this report was to demonstrate that these modelling and numerical techniques could be used to study the transient flame problem which NASA's Lewis Laboratory has been studying experimentally and, furthermore, to demonstrate that a computer code based upon the analytical model and numerical techniques can be developed to give good quantitative as well as qualitative agreement with experiment.

CHAM used its EASI (Elliptic Axisymmetric Integrator) code as a starting point. The specific derivative of this code which was assembled for this project described herein was termed EGOMAC (Effect of Gravity on Methane-Air Combustion)

The program of work has been done in two parts. Firstly EGOMAC was assembled and run for a particular choice of geometry and fuel-supply conditions. When the code was seen to produce qualitatively correct results for the transient flame, the second part of the work was devoted to a systematic investigation of the effects on the computed solutions of:- computational grids; time steps; outer boundary conditions; number of iterations; relaxation factors; and solution order of equations. The code was additionally exercised for two other fuel flow rates, and two other tube diameters. In addition the sensitivity of the solutions to changes in the specified physical chemical constants was also studied.

The remaining two parts of the introductory chapter are devoted to a description of previous work, and to outlining the specific new features embodied in the CHAM approach to this problem. The second chapter describes the mathematical analysis upon which the computer code is based. The third and fourth chapters contain respectively a presentation and

Personnel at CHAM Ltd have been developing numerical models and solution algorithms for predicting axially flowing reacting flows. Patankar and Spalding (Reference 8) describe the GENMIX code which has been widely used for diffusion flames under "parabolic" conditions, i.e. those of steady flow without upstream propagation of influences from downstream.

Edelman et al, concluded that axial diffusion of mass, energy and momentum which introduced "elliptic" effects (i.e. propagation upstream of influences from downstream) becomes important at low-Reynolds-Number, zero-gravity conditions. This indicates an explicit requirement of the analytical method solving the transient laminar flame problem, viz that it should be an elliptic method.

CHAM has developed a basic elliptic code (EASI) which is well suited to this problem, and has therefore used it as the basis for the development of the EGOMAC code which is described in this report.

1.3. Outline of the Present Contribution

The EGOMAC code contains all of the computational advantages contained in the basic EASI code i.e. rapid convergence and accuracy without the excessive computing times usually associated with elliptic codes. The main contribution of the work presented in this report is to demonstrate that the EGOMAC code will efficiently compute the hydrodynamic and thermodynamic fields associated with the laminar flame under transient gravity conditions. This demonstration renders the validity of the novel features embodied into the code self-evident. These novel features include:-

1. Inclusion of axial diffusion in the physical model which in certain cases is the mechanism which keeps the flame alight.
2. Provision of lateral pressure gradients in the model.

3. The use of hybrid differencing scheme to enhance both accuracy and stability.
4. The use of implicit rather than explicit procedures for calculating all variables in the flow field (this is the heart of the SIMPLE Algorithm).

During the study described herein, it should be noted that additional computational efficiency was achieved by ensuring that the initial conditions, corresponding to a 1g steady flame were computed using the GENMIX code. In this way, it was possible to ensure that the transient calculation started from a fully converged and precise definition of all relevant physical quantities. This together with the significance of the novel features contained in the EGOMAC code will be described in more detail in later chapters.

2. MATHEMATICAL ANALYSIS

2.1 Differential Equations and Boundary Conditions

Differential Equations

Equations are solved for the following eight dependent variables :

- the components of velocity in the axial and radial (x and r) directions - u and v,
- the static pressure - p,
- the enthalpy - h,
- the mixture fraction - f - defined as the proportion of fluid present at any point which originated from the nozzle,
- the mass fraction of fuel (methane) - m_{fu},
- and the radiation-flux quantities - R_x and R_r which are defined in terms of the radiative heat fluxes in the positive and negative x direction (K and L) and the positive and negative r direction (I and J), as follows :

$$R_x \equiv \tfrac{1}{2}(K + L) \qquad (2.1\text{-}1)$$

$$R_r \equiv \tfrac{1}{2}(I + J) \qquad (2.1\text{-}2)$$

The conservation equations for most of the above quantities (viz. for all except p, R_x and R_r, which are considered later) are solved in the general form appropriate to an unsteady, axisymmetric flow given below :

$$\frac{\partial}{\partial t}(\rho\phi) + \frac{\partial}{\partial x}\left(\rho u\phi - \Gamma_\phi \frac{\partial \phi}{\partial x}\right) + \frac{1}{r}\frac{\partial}{\partial r}\left[r\left(\rho v\phi - \Gamma_\phi \frac{\partial \phi}{\partial r}\right)\right] = S_\phi$$

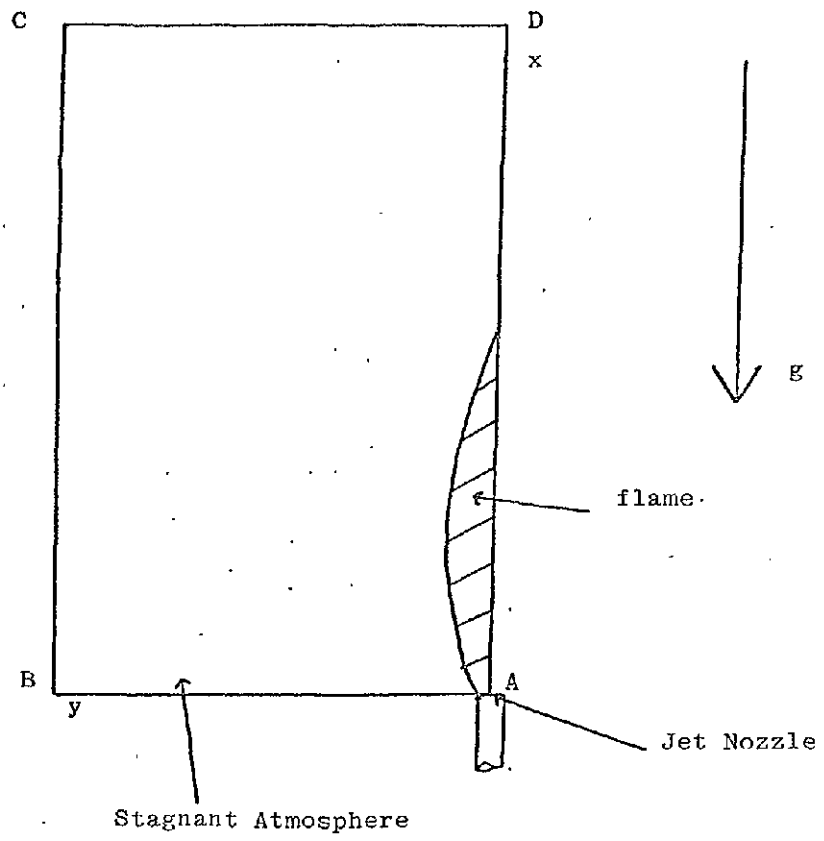

Fig. 2-a: The Domain of Integration

In this equation, t is the time, ϕ is the general dependent variable and ρ is the density.

The diffusion coefficient for ϕ (Γ_ϕ) is evaluated as follows :

For velocities, $\Gamma_\phi = \mu$ (2.1-4)

and, for other variables, $\Gamma_\phi = \mu/\sigma_\phi$ (2.1-5)

Here, μ stands for the laminar viscosity of the fluid (which is calculated as described in Section 2.2 below), and σ_ϕ is the Prandtl or Schmidt number. In the present work, σ_h, σ_f and $\sigma_{m_{fu}}$ are taken to be constant and equal to 0.6, except that for one calculation (case 26) σ_h is set to 0.7.

Values are given in Table 2-a for the source terms S_ϕ. The symbol g there stands for the gravitational acceleration in the negative x direction (see Fig. 2-a). In the source term for h, a is the absorption coefficient, and E is the black-body emissive power, which is related to T (the local absolute fluid temperature) and the Stefan-Boltzmann constant (σ), by :

$$E = \sigma T^4 \qquad (2.1\text{-}6)$$

ϕ	S_ϕ
u	$-\frac{\partial p}{\partial x} + \frac{\partial}{\partial x}\left(\mu \frac{\partial u}{\partial x}\right) + \frac{1}{r}\frac{\partial}{\partial r}\left(r \mu \frac{\partial v}{\partial x}\right) - g\rho$
v	$-\frac{\partial p}{\partial r} + \frac{\partial}{\partial x}\left(\mu \frac{\partial u}{\partial r}\right) + \frac{1}{r}\frac{\partial}{\partial r}\left(r \mu \frac{\partial v}{\partial r}\right) - \frac{2\mu v}{r^2}$
h	$2a(R_x + R_r) - 4aE$
f	0
m_{fu}	$Z \bar{p}^2 m_{fu} m_{ox} \exp(-A/\mathcal{R}T)$

Table 2-a : List of Source Terms

Finally, in the source term for m_{fu} (which is a consequence of presuming that the reaction-rate is given by an Arrhenius expression) Z and A are constants whose values are set as described in Section 3, while m_{ox} is the concentration of O_2.

The pressure p, is deduced, by the method described in Section 2.3, from the mass-continuity relation, which :

$$\frac{\partial \rho}{\partial t} + \frac{\partial(\rho u)}{\partial x} + \frac{1}{r}\frac{\partial}{\partial r}(\rho v r) = 0 \qquad (2.1\text{-}7)$$

Finally, the equations for R_x and R_y are :

$$\frac{d}{dx}\left(\Gamma_{R_x}\frac{dR_x}{dx}\right) + S_{R_x} = 0 \qquad (2.1\text{-}8)$$

$$\frac{1}{r}\frac{d}{dr}\left(r\,\Gamma_{R_r}\frac{dR_x}{dr}\right) + S_{R_x} = 0 \qquad (2.1\text{-}9)$$

where, $$\Gamma_{R_x} = 1/(a+s) \qquad (2.1\text{-}10)$$

$$\Gamma_{R_r} = 1/(a+s+1/r) \qquad (2.1\text{-}11)$$

$$S_{R_x} = a\,E + s\,(R_x + R_r)/2 - (a+s)\,R_x \qquad (2.1\text{-}12)$$

$$S_{R_r} = aE + s(R_x + R_r)/2 - (a+s)R_r \quad (2.1\text{-}13)$$

The symbol s here stands for the scattering coefficient.

Eqns. (2.1-8) and (2.1-9), it should be observed, can be regarded as especially simple forms of the general ϕ equation (Eqn. (2.1-3); they lack the time derivative (since radiation is not stored), the convection terms (since radiation is not conveyed by bulk movement), and the diffusion term in the direction normal to that of the radiation flux.

Boundary Conditions

The solution domain is shown in Fig. 2-a. Boundary conditions are applied at all four boundaries as described below.

At the nozzle, the rate of mass inflow is specified; the axial-velocity u profile is parabolic, and the radial velocity (v) is zero. The mixture fraction f is unity by definition; and when, as in the case here, the incoming fluid is pure methane, $\dot{m}_{fu}$ is also unity. The enthalpy h is calculated from the specified fluid temperature as described in Section 2.21.

At the remainder of the lower (AB) boundary, and at the outer (BC) boundary, h is deduced from the specified ambient temperature; u, f and m_{fu} are zero at both boundaries, and the lateral velocity v is zero at the lower boundary. At the outer (BC) boundary, the v velocities are set so as to account for the lateral mass inflow by entrainment.

The distribution of mass inflow was previously determined

from solutions with the boundary-layer procedure, GENMIX (Ref. 8), and is tabulated below. However, it is important to remark that, for the calculations reported, the outer boundary was chosen to be sufficiently remote from the flame, that the effect of the conditions prescribed there on solutions within the flame was negligible.*

x cm.	ψ kg.s^{-1}
0.00	0
0.40	1.64×10^{-6}
0.90	4.10×10^{-6}
2.10	9.56×10^{-6}
3.18	1.44×10^{-5}
4.46	1.95×10^{-5}
5.08	2.18×10^{-5}
6.49	2.65×10^{-5}
7.27	2.92×10^{-5}
8.26	3.24×10^{-5}
9.40	3.57×10^{-5}
20.70	3.96×10^{-5}
12.20	4.38×10^{-5}
13.90	4.83×10^{-5}
15.90	5.35×10^{-5}

Table 2-b : Entrainment mass flow per radian (ψ) at the outer (BC) boundary.

* This was confirmed by tests in which the mass flows were changed to three times the values tabulated.

At the upper boundary (where outflow occurs), and at the symmetry axis, the lateral velocity (v) is zero, and the inwardly-directed flux of u, h, m_{fu} and f is zero.

Finally, the boundary conditions for R_x and R_y at the symmetry axis are deduced from the knowledge that the net radiative heat transfer across the axis of symmetry is zero; elsewhere the presumption is that outgoing radiation escapes without reflection, while the incoming radiation is σT_b^4, where T_b is the temperature of the fluid at the boundary.

2.2 Auxiliary Inputs

2.2.1 Thermodynamic Functions

The enthalpy (h) is calculated as follows :

$$h = \Sigma h_j m_j + H\, m_{fu} \qquad (2.2\text{-}1)$$

where H is the lower value of the heat of formation of methane; the value used here is $H=4.10^7$ J/kg. The summation sign denotes summation over all species present. The species enthalpies h_j are defined as follows :

$$h_j \equiv \left(C_{j0} + C_{j1}T + C_{j2}T^2 + C_{j3}T^3 \right) T \qquad (2.2\text{-}2)$$

The coefficients C_j are tabulated in Table 2-C.

Species	$C_{jo} \times 10^{-2}$	$C_{j1} \cdot \times 10^{-2}$	$C_{j2} \cdot 10^{-4}$	$C_{j3} \cdot 10^{-8}$
	(J/kg)	(J/kg^{O}K)	(J/kg^{O}K^{2})	(J/kg^{O}K^{3})
N_2	10.435	-5.3981	1.2784	-3.3472
O_2	8.7061	15.800	-0.21869	-0.13947
CO_2	6.4748	70.181	-3.2833	5.8576
H_2O (Vapour)	18.343	0.019232	2.7700	-7.2523
CH_4	15.0995	212.57	-1.8268	-8.3016

Table 2-C : The values of the C_j in Eqn. (2.2-2)

The species concentrations in Eqn. (2.2-1) are deduced as described in Section 2.24 below.

2.2.2 The Calculation of Viscosity

The local mixture viscosity (μ) is determined from the following formula :

$$\mu = m_{O_2} \mu_{O_2} + m_{CH_4} \mu_{CH_4} + \left(m_{H_2O} + m_{CO_2} + m_{N_2}\right) \mu_{N_2} \qquad (2.2\text{-}3)$$

Here, it will be observed, the combustion products are lumped together with the nitrogen; the error in μ introduced by this practice will be small when, as is the case here, the nitrogen is present in larger quantities than H_2O and CO_2. In any case, the viscosities of H_2O and CO_2 are not markedly different from that of N_2.

The viscosities μ_{fu}, μ_{ox} and μ_{N_2} are related to the local temperature via Sutherland's Law, which is :

$$\mu_i = A_i T^{3/2} / (B_i + T) \qquad (2.2\text{-}4)$$

The coefficients A_j and B_j are tabulated below :

Species	$A_j \times 10^6$ (kg/msec$^\circ K^{1/2}$)	B_j ($^\circ K$)
CH_4	1.00490	171.473
O_2	1.74410	144.207
N_2	1.40510	111.452

Table 2-d : The coefficients in Sutherland's viscosity law - Eqn. (2.2-4).

2.2.3 The Calculation of Density

The local gas density (ρ) is calculated from the perfect-gas law :

$$\rho = \bar{P} / \{ \mathcal{R} T \sum_j (m_i / M_i) \} \qquad (2.2\text{-}5)$$

where $\bar{p}$ is the mean fluid pressure, presumed for the present calculation to be that of the ambient surroundings; R is the universal gas constant; and M_j is the molecular weight of species j. The summation is over all species present.

2.2.4 The Chemical-reaction Models

The chemical reaction considered is:-

$$CH_4 + 2O_2 \longrightarrow 2H_2O + CO_2$$

The reaction is presumed to be irreversible, and to occur in a single step.

Two reaction models have been employed. The first presumes that the rate of reaction is infinite; fuel and oxygen therefore cannot coexist. When this is so, there is no need to solve the transport equation for m_{fu}; both m_{fu} and m_{ox} may be deduced from the mixture fraction f as follows* :

If $0 \leqslant f \leqslant f_{st}$:

$$m_{fu} = 0 \quad , \quad m_{ox} = m_{ox,\infty}\left(1 - \frac{f}{f_{st}}\right) \qquad (2.2\text{-}6)$$

If $f_{st} \leqslant f \leqslant 1$:

$$m_{ox} = 0 \quad , \quad m_{fu} = \frac{f - f_{st}}{1 - f_{st}} \qquad (2.2\text{-}7)$$

Here, $m_{ox,\infty}$ is the mass fraction of oxygen in the ambient air, and f_{st}, the mixture fraction for a stoichiometric mixture, is :

---

* These formulae, and others given later in this section, presume that m_{fu} at the jet is unity; i.e. the jet is composed of pure methane.

$$f_{st} = 1/\left(1 + i/m_{ox,\infty}\right) \qquad (2.2\text{-}8)$$

where, i is the mass of oxygen needed just to burn unit mass of fuel to completion; for the reaction considered here, therefore, i = 4.

The above formulae are depicted graphically in Fig. 2-b, which shows the variation of m_{fu}, m_{ox} (and also m_{N_2}, m_{H_2O} and M_{CO_2} with mixture fraction f.

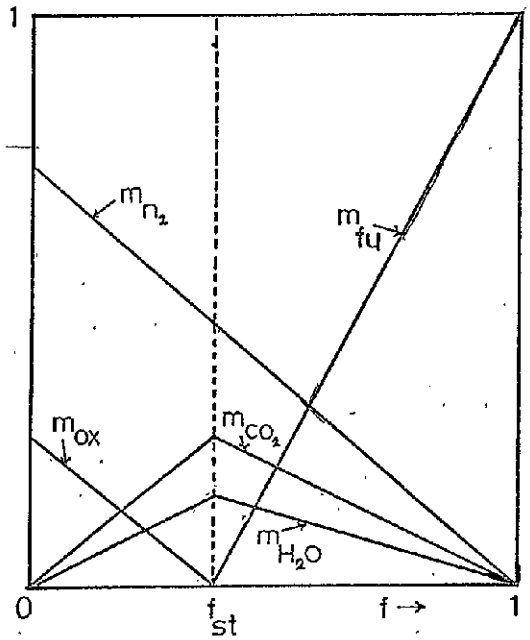

Fig. 2-b : Variation of species concentrations with f for an infinitely-fast reaction.

In the second reaction model, the rate of reaction is calculated from an Arrhenius expression. The transport

equation for m_{fu} given in Section 2.1 is solved, and m_{ox} is computed from :

$$m_{ox} = (1 - f)\, m_{ox,\infty} - i(f - m_{fu}) \qquad (2.2\text{-}9)$$

For both reaction models, the following formulae are employed for calculating the remaining species concentrations :

$$m_{H_2O} = (f - m_{fu}) \cdot 2 \frac{M_{H_2O}}{M_{fu}} \qquad (2.2\text{-}10)$$

$$m_{CO_2} = (f - m_{fu}) \cdot \frac{M_{CO_2}}{M_{fu}} \qquad (2.2\text{-}11)$$

$$m_{N_2} = 1 - m_{fu} - m_{ox} - m_{CO_2} - m_{H_2O} \qquad (2.2\text{-}12)$$

2.3 The Solution Method

2.3.1 The Finite-Difference Equations

The equations are solved by a marching-integration finite-

difference method, based on the work of Patankar and Spalding (Ref. 9), in which the domain of solution in the x-r plane is imagined to be covered by a mesh of grid points as shown below* :

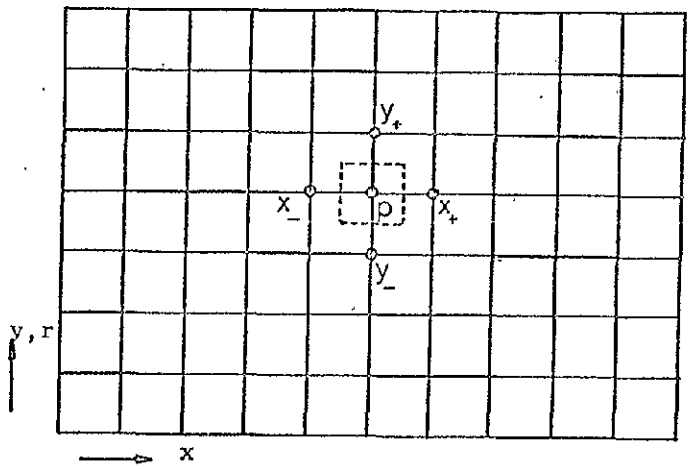

Fig. 2-c : The finite-difference grid.

The value of ϕ at grid point P and at a particular time t^n is related to the value at P at the previous time step (ϕ_P^o), and to the values at the neighbouring grid points X+, X-, Y+ and Y-, by integrating the general ϕ equation (Eqn. (2.1-3)) over the small control volume or cell surrounding P shown in Fig. 2-c. For performance of the integration, realistic assumptions are made regarding the variations of ϕ in the x, y and t directions between grid nodes; for most purposes the variations are taken to be stepwise. The convective and diffusive fluxes are, however, calculated using a special hybrid difference scheme, due to Spalding (Ref. 10), which is designed to improve accuracy

---

* Because the general solution method described here is valid for Cartesian (x,y) coordinates as well as the cylindrical coordinates used here, the symbol y is often used throughout this section to refer to the radial direction.

and to eliminate instabilities which can occur when the convection terms are large compared with the diffusive ones. The $\partial(\rho\phi)/\partial t$ term is evaluated on the presumption of linear variation of ϕ with t; for all other purposes, the new values of ϕ are assumed to prevail over the whole of time range t^o to t^n.

The outcome of the integration is a finite-difference equation of the form :

$$A_P \phi_P = A_{x+} \phi_{x+} + A_{x-} \phi_{x-} + A_{y+} \phi_{y+} + A_{y-} \phi_{y-} + A_P^o \phi_P^o + S_u \qquad (2.3\text{-}1)$$

in which equation the coefficients A_{x+}, A_{x-}, A_{y+} and A_{y-} contain the effects of convection and diffusion, while A_p^0 accounts for the unsteady term. The integral source term has been written in the linearised form $S_u + S_p\phi_p$*, and the coefficient S_p has been combined into A_p, which is defined as :

$$A_P = A_{x+} + A_{x-} + A_{y+} + A_{y-} + A_P^o - S_P \qquad (2.3\text{-}2)$$

The velocities are treated, in two respects, differently from other variables. Firstly, the velocity grid points are located midway between the nodes for other variables. This arrangement, which is illustrated in Fig. 2-d, has the convenient feature that the velocities are stored midway between the pressures which drive them. The second special feature of the velocity equations, is that, in preparation for the calculation of pressure by the means described in

---

*Footnote : The use of this form, when S_p is negative, is often found to enhance the stability of the solution; for, when (S_p) is large, equation (2.3-1) tends to :

$$\phi_p[A_p^0 + (-S_p)] = A_p^0 \phi_{p_0}$$

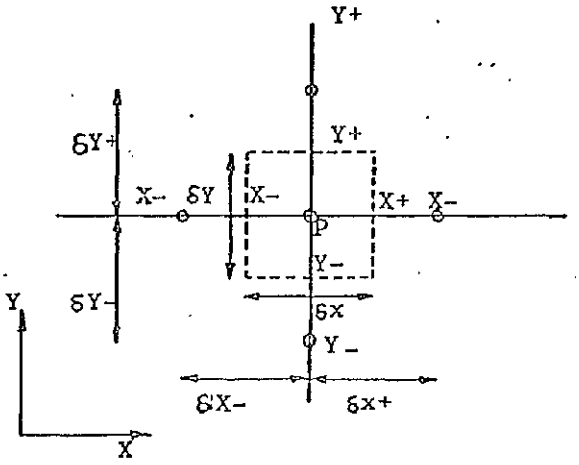

Fig 2-d: A typical finite-difference cell

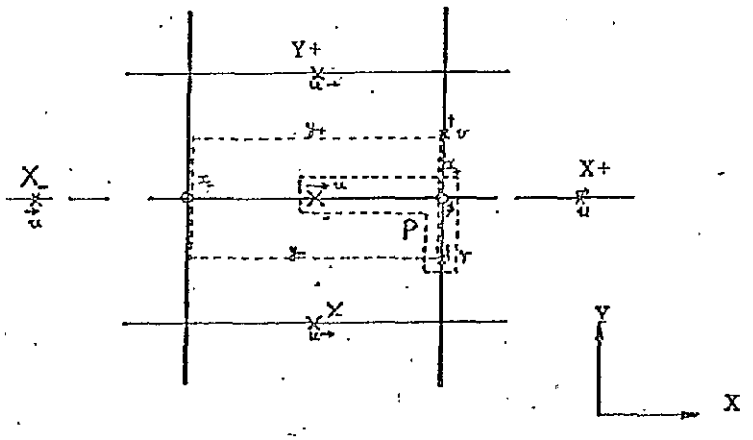

Fig 2-e: Velocity grid nodes

the next section, the pressure-gradient part of the source term is separated from the rest. The finite-difference equation for u, for example, therefore has the form :

$$A_P u_P = A_{x+} u_{x+} + A_{x-} u_{x-} + A_{y+} u_{y+} + A_{y-} u_{y-} + A_P^\circ u_P^\circ + S_u + D_P^u (P_{x-} - P_P) \quad (2.3\text{-}3)$$

The subscript nomenclature adopted for the velocities is illustrated in Fig.(2.3-3). Thus, P refers to variables stored at nodes within the boomerang-shaped envelope in the figure.

Finite-difference equations may be derived for R_x and R_y, in a similar manner to that for ϕ by integration of Eqns. (2.1-8) and (2.1-9).

The resulting equations have the form :

$$A_P R_{xP} = A_{x+} R_{x,x+} + A_{x-} R_{x,x-} + S_u \quad (2.3-4)$$

$$A_P R_{yP} = A_{y+} R_{y,y+} + A_{y-} R_{y,y-} + S_u \quad (2.3-5)$$

2.3.2 The calculation of pressure

Pressure is calculated by a novel procedure due to Patankar and Spalding (Ref. 9), which at each time-step the momentum equations are first solved for an estimated pressure field, which is subsequently corrected so as to ensure that the corrected velocity field satisfies mass continuity for each cell. This is achieved as described below.

The finite-difference form of the mass-conservation equation

may be written as :

$$\frac{(\rho_P - \rho_P^o)}{(t^n - t^o)} \delta x \delta y + a_{x+} \rho_x u_{x+} - a_{x-} \rho_x u_P + a_{y+} \rho_{y+} v_{x+} - a_{y-} \rho_{y-} v_P = 0 \qquad (2.3\text{-}4)$$

where δx and δy are all dimensions, and a_x, a_{y+} and a_{y-} refer to cell face areas. All these quantities are shown in Fig. 2-c.

The velocity corrections (u' and v') can be related by the following approximate linear relations to the pressure corrections (p') :

$$u'_P = E^u_P (P'_{x-} - P'_P) \qquad (2.3\text{-}5)$$

$$v'_P = E^v_P (P'_{y-} - P'_P) \qquad (2.3\text{-}6)$$

In steady-state calculations, the coefficients E^u_p and E^v_p are simply set equal to D^u_p/A_p and D^v_p/A_p. For transient calculations, however, a stability-enhancing form* is used, in which E^u_p, for example, is set to D^u_p/A^o_p.

The steady-state version, in contrast, presumes that $u_{x+} = u'_{x-} = u'_{y+} = u'_{y-} = 0$.

Substitution of these expressions (and similar formulae for u'_{x+} and u'_{y+} into Eqn. (2.3-4), yields an equation for the pressure correction p', of the following form :

---

*Footnote : Which results from presuming that in a transient flow in which changes are taking place systematically, it is reasonable to suppose that:

$$u'_{x+} \simeq u'_{x-} \simeq u'_{y+} \simeq u'_{y-} \simeq u'_P$$

$$A_P p'_P = A_{x+} p'_{x+} + A_{x-} p'_{x-} + A_{y+} p'_{y+} + A_{y-} p'_{y-} - M_P \qquad (2.3\text{-}7)$$

where m_p is the mass source at P associated with the velocity field (u* and v*) calculated from the estimated pressures; i.e. :

$$M_P = \frac{(\rho_P - \rho_P^o)}{(t^n - t^o)} \delta x \delta y + a_x \rho_{x+} u^*_{x+} - a_x \rho_{x-} u^*_P + a_{y+} \rho_{y+} v^*_{y+} - a_{y-} \rho_{y-} v^*_P \qquad (2.3\text{-}8)$$

2.3.3 Solution of the Equations

The overall solution scheme is as follows; at each time step, the following operations are performed :-

(i) The first operation is to calculate the fluid properties μ and ρ at each grid node, from the temperatures at the previous time step.

(ii) The momentum equations are then solved for the estimated pressure (p*) field, to yield u* and v*. The p*'s are usually taken as equal to p^o.

(iii) Next, the p' equations are solved, and the appropriate corrections are applied to the pressures and velocities, according to Eqns. (2.3-5) and (2.3-6).

(iv) Finally, the equations are solved for the remaining ϕ's.

In some cases (detailed in Section 3), the practice was adopted of iterating on u, v and p by repeating steps (ii) and (iii) several times, and using, for all iterations but the first, the calculated pressures at the previous iteration as the estimated pressure field.

Finally, it should be remarked that the sets of finite-difference equations of the form of Eqn. (2.3-1) are solved by the fast alternating-direction TDMA method described in Ref. 9.

2.3.4 The Provision of Steady-state Solutions.

The initial conditions of the zero-gravity transient calculations, were solutions obtained for the steady-state situation with gravity for the same conditions. For these steady-state calculations, it is of course desirable to employ realistic initial guesses to the fluid-property fields; in particular, high initial temperatures must be provided in the region of the flame, in order to ensure that ignition occurs. For the computations reported here, the initial conditions for the steady-state solutions were calculated by presuming parabolic profiles of u and uniform profiles of all other quantities within the flame (Fig. 2-f). The overall balance equations for mass, momentum, mixture fraction and enthalpy for the conical-shaped flame are then :

$$\frac{\bar{\rho}\,\bar{u}\,R^2}{2} = \left(\frac{\bar{\rho}\,\bar{u}\,R^2}{2}\right)_o + \Psi \qquad (2.3\text{-}1)$$

$$\frac{4}{3}\,\frac{\bar{\rho}\,\bar{u}^2\,R^2}{2} = \frac{4}{3}\left(\frac{\bar{\rho}\,\bar{u}^2\,R^2}{2}\right)_o \qquad (2.3\text{-}2)$$

$$\frac{\bar{\rho}\,\bar{u}\,R^2\,\bar{f}}{2} = \left(\frac{\bar{\rho}\,\bar{u}\,R^2}{2}\right)_o \qquad (2.3\text{-}3)$$

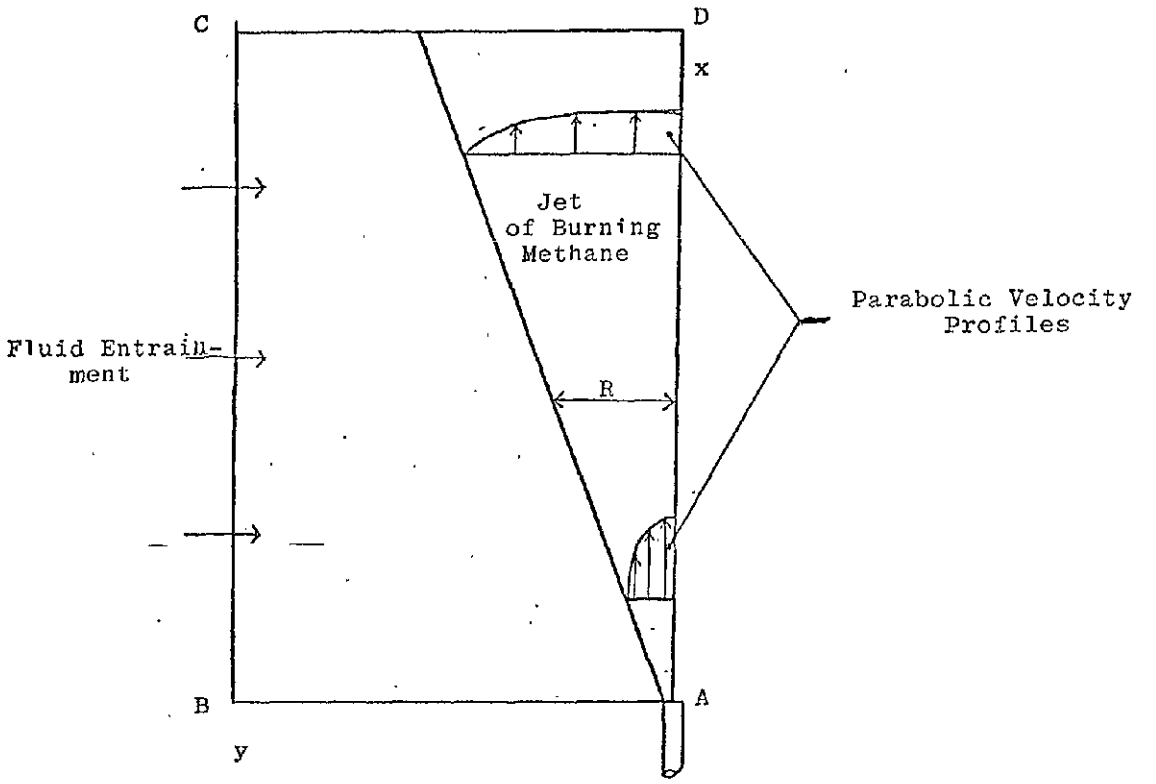

Fig 2-f: Starting Conditions.

$$\bar{\rho}\frac{\bar{u}\,R^2\,\bar{h}}{2} = \left(\bar{\rho}\frac{\bar{u}\,R^2\,\bar{h}}{2}\right)_o + \psi h_\infty \qquad (2.3\text{-}4)$$

Here, the overbar denotes mean values within the flame, and subscript o refers to conditions at the nozzle; ψ is the entrainment mass flow given in Table 2-b.

These equations are solved, assuming infinite reaction rate, to yield R, $\bar{u}$, $\bar{h}$ and $\bar{f}$, which provide initial values for u, h , and T. The pressure is presumed uniform, initially, at atmospheric pressure, and v is set so as to satisfy local continuity.

Furthermore, when the m_{fu} equations were solved, a steady-state solution for infinite reaction rate was used so as to provide initial conditions for the finite-reaction-rate calculations.

2.4 The Computer Program

The calculations have been performed with a version of the CHAM computer code, EASI (the name stands for elliptic axisymmetric integrator), which is a general computer program, written in Fortran IV, for calculating flow and heat and mass transfer in two dimensional flow with or without re-circulation. Both unsteady and steady flows may be handled, and the solution may be performed in cartesian or cylindrical-polar coordinates.

3. DETAILS OF THE COMPUTATIONS

3.1. Introduction

Task II of the contract required performance of computations for 25 different cases to assess the capability and accuracy of the solution procedure. Some of these cases were devised to illuminate the effects of certain parameters of the numerical procedure, such as the number of grid points, time step and under-relaxation factors. Other cases investigated the response of the solution to variations in the experimental conditions or the reaction-rate constants.

In the course of carrying out the computations, and due to the lack of experimental data concerning the reaction-rate constants, it was decided to perform computations for some additional cases. In fact a total of 21 extra cases were studied, bringing the total number of cases to 46. The specifications of all these cases are presented below.

3.2. Specifications of the Cases Studied

Case 0

The experimental conditions of this case are those specified in Task I of the contract and thus the label 'standard case' will be used later in the report to refer to this case.

Case 1

The number of grid nodes was decreased by 51% from that of Case 0.

Case 2

The number of grid nodes was increased by 40% from that of Case 0

Case 3

The standard time-step (.01 sec.) was decreased by a factor

of 3 for the first 0.4 sec. of the transient solution.

Case 4

The standard time-step was decreased by a factor of 10 for the first 0.4 sec. of the transient solution.

Case 5

The standard time-step was decreased by a factor of 50 for the time interval starting at .01 sec. and ending at 0.308 sec.

Case 6

The standard time-step was increased by a factor of 10 throughout the interval of zero to 1 sec.

Case 7

The position of the cylindrical boundary BC (Fig.1) was moved outward by 50% of the standard value. The converged steady-state (1-g) solution for the standard case was read off disk and employed as the starting conditions for this case, except that the velocities along the cylindrical boundary were appropriately modified to ensure the same fluid entrainment for both this case and the standard case.

Case 8

The position of the cylindrical boundary, BC was moved inward by 50% of the standard case.

Case 9

The number of iterations, at each time step, on the hydrodynamic variables u,v,p were doubled. Previously, only one iteration was performed during the transient solution.

Case 10

As for 9 except that the hydrodynamic variables were iterated upon four times.

Case 11

This case examines the effect on the transient solution of under-relaxing the dependent variables. The following formula for under relaxation was used to calculate the value of a dependent variable ϕ_p :

$$\phi_p = (1-\alpha)\phi_p^\circ + \alpha\phi_p$$

where ϕ_p and ϕ°_p are the values of ϕ at the current and previous time-steps respectively, and α is the under-relaxation factor. The value of α was taken as 0.5 for all variables.

Case 12

As for case 11 except that the value of α was decreased to .25

Case 13

The order of solution of the finite-difference equations was altered as shown in table (3-b).

Case 14

A further change of the solution order was made as shown in table (3-b).

Case 15

The fuel flow-rate was reduced to 1.08 cm^3/sec. The longitudinal length, X_1, of the integration domain was reduced to 4 cm to accommodate appropriately the shorter flame. This adjustment of X_1 was based on the analytical solution of a constant-property laminar diffusion flame that predicts that the flame length is proportional to the flow rate. The hydrodynamic variables U, V, P were iterated upon twice to smooth out the solution.

Case 16

As for case 15 except the fuel flow rate was increased to

5.15 cm^3/sec and the value of X_1 was correspondingly adjusted.

Case 17

Both the mass flow-rate and the nozzle diameter were increased as shown in table (3-a). The longitudinal length, X_1, of the integration domain was estimated as discussed earlier. The radial width, Y_1, of the domain was also estimated from the constant-property analytical solution, which predicts that the maximum flame width is proportional to the nozzle diameter.

The contract required that for this case, the converged solution of the steady (1-g) condition be obtained and used as the initial condition for the following unsteady case.

Case 18

The experimental conditions for this case were the same as of Case 17 except that here the gravity was zero.

Case 19

The fuel flow-rate was smaller than that of Case 18 but the nozzle diameter was increased as given in table (3-a).

Case 20

The fuel flow-rate and the nozzle diameter were both smaller than those of case 19.

Cases 21 to 25

In the previous 20 cases, the infinite-rate reaction model (section 2) was employed to obtain the local mass fractions of fuel, oxidant and products. This model, because it assumes that reaction will always take place whenever fuel and oxidant co-exist locally, cannot predict the flame extinction which

occurred experimentally* in Case 20. Thus, in order to predict this extinction, we must employ the finite-rate reaction model (Section 2.24), provided that the appropriate values of the constants A and p are known. Since there was no suitable information to assist in ascribing the values of A and p these quantities could be treated as parameters that could be freely varied until the desired solution was obtained. The converged (1-g) infinite-rate solution was taken as a starting point; this corresponds to A=0. Then successively increasing values of A were employed (Cases 22A to 22I), in a search for the critical value of A which just kept the (1-g) flame alight. The idea was that the transient solution would predict the flame extinction if the critical value of A was employed. Cases 24A to 24I were also performed in the search for the critical value of A within a wider range. Although this critical value of A was not obtained in the few runs which were made, valuable experience was gained and will be reported upon.; it establishes necessary foundation for future use of the solution procedure.

The values of A used in Cases 21 to 25 are listed in table (3-C).

The purpose of Case 21 was to demonstrate that the finite-rate model when employed with a sufficiently small value of A (i.e. very fast reaction) will produce results which are consistent with those of the infinite-rate model.

Cases 23 and 25 are both for the transient study of two different values of A, namely 10^4 and 1.5×10^4.

It can be seen from table (3-C) that the temperature was under-relaxed in Cases 21, 24A to 24I and 25. This practice was necessary to dampen the oscillations of temperature as

---

*This information was received through a telephone call from Dr. Cochran.

will be discussed later.

Case 26

In this case, the Prandtl number, σ_h was increased to 0.7 to examine its effect on the solution by comparing the results with those of the standard case where σ_h was 0.6.

After presenting the specifications of the studied cases, we can proceed now to discuss the results.

Case	Experimental conds.		Size of Integration domain		Time-Step Information		
	Flow Rate (cm^3/sec)	Nozzle Dia (cm)	X_1 (cm)	Y_1(cm)	Δt (secs)	t_o(secs)	t_1(secs)
0	2,8	.102	8.	4.5	.01	0.	1.
1	"	"	"	"	"	"	"
2	"	"	"	"	"	"	"
3	"	"	"	"	.003) .01)	0. .4	0.4) 1.)
4	"	"	"	"	.001) .01)	0.0 0.4	0.4) 1.)
5	"	"	"	"	.01) .0002)	0.0 0.01	.01) .308)
6	"	"	"	"	0.1	0.0	1.
7	"	"	"	6.75	.01	0.0	1.
8*	"	"	"	2.25	"	"	"
9	"	"	"	4.5	"	"	"
10	"	"	"	"	"	"	"
11	"	"	"	"	"	"	"
12	"	"	"	"	"	"	"
13	"	"	"	"	"	"	"
14	"	"	"	"	"	"	"
15	1.08	"	4.	"	"	"	"
16	5.15	"	15.	"	"	"	"
17&18	5.50	.165	15.	7.5	"	"	"
19	3.20	.884	12.	40.	"	"	"
20	2.42	.372	8.	20.	"	"	"
21	2.8	.102	8.	4.5	.01	0.	1.03
22A-I	2.42	.372	8.	20.	.01	0.0	1.
23	"	"	"	"	"	"	"
24A-M	"	"	"	"	"	"	"
25	"	"	"	"	"	"	"
26	2.8	.102	8.	4.5	.01	0.	1.03

*Error in Computation

Table (3-b)

Case	Grid*	Number g Iterations per time-step	Under-relaxation factors for dependent variables	Solution Order of Dependent variables.
0	17 x 25	1	1.0	u,v,p,h,f,R_x,R_y
1	12 x 18	"	"	"
2	24 x 25	"	"	"
3	17 x 25	"	"	"
4	"	"	"	"
5	"	"	"	"
6	"	"	"	"
7	"	"	"	"
8	"	"	"	"
9	"	2	"	"
10	"	4	"	"
11	"	1	0.5	"
12	"	"	0.25	"
13	"	"	1.0	v,u,p,f,h,R_y,R_x
14	"	"	"	R_x,h,R_y,f,v,u,p
15	"	2	"	u,v,p,h,f,R_x,R_y
16	"	"	"	"
17	"	"	"	"
18	"	"	"	"
19	"	"	"	"
20	"	"	"	"
21	"	1	"	"
22A-I	"	-----	"	"
23	"	1	"	"
24A-M	"	-----	"	"
25	"	1	"	"
26	"	"	"	"

*In all cases, the grid lines were non-uniformly spaced. A geometrical progression was employed in both the x-and y-directions.

Table (3-c)

Case	Arrhenius Constant A (J/Kg mol/^{o}K)	Number of Iterations at each storage	Under-relaxation factor for temperature	Transient Studied?
21	10.	80	= 3	Yes
22 A	10,000	10	= 1	No
B	11,000	"	"	"
C	12,000	"	"	"
D	13,000	"	"	"
E	14,000	"	"	"
F	15,000	"	"	"
G	16,000	"	"	"
H	17,000	"	"	"
I	18,000	"	"	"
23	10,000	50	= 1	Yes
24 A	10.	100	= 3	No
B	5,000	20	"	"
C	8,000	"	"	"
D	10,000	"	"	"
E	11,000	"	"	"
F	12,000	"	"	"
G	13,000	"	"	"
H	14,000	"	"	"
I	15,000	"	"	"
J	16,000	"	"	"
K	17,000	"	"	"
L	18,000	"	"	"
M	19,000	"	"	"
25	15,000	100	= 3	Yes

*For cases 22 and 24, a stage refers to a new value of A, while it denotes the steady (1-g) condition for cases 21,23 and 25.

Table (3-d)

Case	Prandtl/Schmidt numbers of the variables					
	u	v	p	h	f	m_{fu}
0 - 25	1.	1.	1.	.6	.6	.6
26	1.	1.	1.	.7	.6	.6

4. ANALYSIS AND DISCUSSION OF THE RESULTS

4.1. Introduction

In this chapter, the results of the computations are presented and discussed by the aid of figures 4-a to 4-i and by reference to the attached computer print-outs.

All figures, except Fig. 4-h, compare the variation with time in zero gravity of the flame length for the particular Cases studied.

From considerations of dimensional analysis, discussed in detail in Chapter 5, it was found that the transient behaviour of the flame can be best studied by expressing the flame length and time in a dimensionless form as $\tilde{x}_{fl}$ and $\tilde{t}$ respectively.

The definitions of $\tilde{x}_{fl}$ and $\tilde{t}$ are:

$$\tilde{x}_{fl} \equiv \left[\frac{x_{fl}}{D_c}\right]\left[\frac{\mu_\infty}{D_c \rho_0 u_0}\right]$$

$$\tilde{t} \equiv \left[\frac{2tu_0}{D_c}\right]\left[\frac{\mu_\infty}{D_c \rho_0 u_0}\right]$$

Here, x_{fl} is the flame length defined as the distance along the axis of the fuel nozzle where the mixture-fraction f is equal to f_{st} .

4.2. Results and Discussion

4.2.2 Grid dependence

The dependence of the solution on the number of grid points in the integration domain, is illustrated here by way of the variation of $\tilde{x}_{fl}$ with $\tilde{t}$. This is done for the

three Cases 0, 1 and 2. The experimental conditions for these cases are identical. The finite-difference grids of the cases are 17 x 25, 12 x 18 and 24 x 25 respectively.

Figure 4-a displays the transient behaviour of $\tilde{x}_{fl}$ for the three grids. It is demonstrated that for a fixed time-step increasing the number of grid points in the domain of integration (i.e. refining the grid) leads to larger oscillations of the predicted flame-length . These oscillations may be linked with the numerical instability caused by the relatively large magnitude of the convection and diffusion terms as compared to the transient in the finite-difference equation when the time-step is large.

4.2.2.Effect of variation of the time step

Four Cases (0, 3, 4 and 6) are chosen to demonstrate the dependence of the solution on the value of the time step. These cases have the same experimental conditions; and the parameters that affect the numerical solution are identical except for the time step. The time steps for the four cases are .01, .003, .001 and .1 sec. The variations of $\tilde{x}_{fl}$ with $\tilde{t}$ for these cases are compared in fig. 4-b.

It is indicated in the figure that as we decrease the time step (Cases 3 and 4), the oscillations of the predicted $\tilde{x}_{fl}$ are dampened. The result of Case 5 (time step = .0002 sec) is not plotted in this figure, since the variation of $\tilde{x}_{fl}$ is almost identical to that of Case 4. One may, however, compare the respective print-outs of Cases 4 and 5 after a time of 0.03 sec. It will then be clear that further refinements in the time step have insignificant effects on the solution.

The band of the experimental results is also shown in fig.4-6. The predictions of cases 3 and 4 are seen to be in fair agreement.
On the other hand, when the time step becomes very coarse(Case 6) large deviation from the meansurements is observed.

4.2.3.Effect of varying the lateral width of the integration domain

The influence of increasing the lateral width, Y_1, of the integration domain, is shown by Fig. 4-c, where the transient behaviour of $\tilde{X}_{fl}$ is plotted for the two cases 7 and 0. In Case 7, Y_1 is 50% greater than that of Case 0. It is illustrated in the figure that the transient variation of $\tilde{X}_{fl}$ for Case 7 differs slightly from that of Case 0.

We can compare the (1-g) flame-lengths from the respective print-outs of both cases. It is indicated that in Case 7, the flame length is 3.8 cm which is about 5.5% longer than that of Case 0 (3.6 cm).

In the attempt of performing the computation for Case 8 which examines the effect of decreasing Y_1, a programming error occured in specifying the radial distance between the 7th and 8th y-grid lines; the radial distance from the axis of symmetry of the 8th line was less than that of the 7th. This error produced an unrealistic result: the flame length after 1 sec in (0-g) became about 63% longer than that of Case 0 (both cases have the same experimental conditions). The location of the error is marked in the respective print-out.

It is expected, however, that when the grid is specified properly, a reduction in the value of Y_1 will produce only slightly different results from that of Case 0.

4.2.4.Effect of iterating at each time step

Here we compare the transient $\tilde{x}_{fl}$ of three Cases (0, 9 and 10) which differ only in the number of iterations performed at each time step. Figure 4-d displays the results of the three cases. Two conclusions can be drawn.

First, it is shown in the figure, and confirmed by the respective print-outs, that increasing the number of iterations from 1 to 2 eliminates the oscillations in the transient flame-length.

Secondly, it is clear that doubling the number of iterations from 2 to 4 produces identical results.

It is interesting to note that the effect on the transient $\tilde{x}_{fl}$ of iterating at each time step is almost the same as that of decreasing the time step (see figures 4-b and 4-d). It should be pointed out, however, that iterating twice at each time step is more economic than halving the time step since iteration applies only to the three dependent variables u, v and p whereas the finite-difference equations are solved for all variables at each time-step.

4.2.5.Effect of under-relaxation during the transient solution

Three Cases (0, 11 and 12) are considered to study the effect of under-relaxing the dependent variables during the transient mode of the solution. Again, the behaviour of $\tilde{x}_{fl}$ is chosen to illustrate the sensitivity of the solution to the changes of the under-relaxation factor α (see section 3-2, Case 11).

Figure 4 - e compares the transient $\tilde{x}_{fl}$ for cases 0 and 11 where the values of α are 1 and .5 respectively. As compared to case 0 (α = 1), Case 11 shows that the time-rate of change of $\tilde{x}_{fl}$ is much smaller, and gradually decreases as we march in time.

Of the three values of α tested, the smallest (.25), case 12 produces hardly any change in the flame length as time increases (see the print-out). Although it is expected that under-relaxation will slow down, to a certain extent, the progress of the redevelopment of the transient behaviour, the predictions show severe slowing down. The cause requires further investigation.

4.2.6. Effect of changing the order of solving the equations

Here we examine the results of changing the order of solving the finite-difference equations of the dependent variables. The behaviour of the transient flame-length for the Cases 0, 13 and 14 is displayed in Fig 4-f. The order of solving the equations in each case is given in table (3-b) and also in Fig. 4-f.

The order of solution in Case 13 differs from that in Case 0 in three respects: the equation of v is solved before that of u, the equation of f is solved before that of h, and the equation of R_y is solved before that of R_x. Figure 4 exhibits identical predictions for the transient in the two cases.

Now let us consider Case 14 and Case 0. In Case 14, the equations of R_x, h, R_y and f are solved before those of v, u and p, whereas in Case 0, the equations of u, v and p were solved before the other four. The result of this difference is displayed in Fig 4-f. It is shown that the transient flame-length in Case 14 is lagging, but otherwise identical to, that of Case 0. This is a consequence of the fact that the flame length was determined (see Section 4.1) from the values of the mixture fraction, f, which in Case 14 was solved for prior to the hydrodynamic variables. The values of f, would be appropriate to the flow field (i.e. convection and diffusion) associated with the previous time-step. Thus,

for example , after the first time step (.01 sec) of the transient mode, the flame length is that corresponding to the (1-g) steady state conditions.

We can then conclude that the solution algorithm is stable with respect to interchanges in the order of solving the finite-difference equations.

4.2.7.Effect of varying the flow conditions

All the Cases (0 to 14) which have been examined up to this point, had the same flow conditions (i.e. the same nozzle diameter, 0.102 cm, and s me methane flow-rate, 2.8 cm^3/sec). Now the effect of varying these conditions is studied by comparing the results, $\tilde{x}_{fl}$ vs. $\tilde{t}$, of six Cases (15 to 20). The results of 3 Cases (15, 16 and 18) are plotted in Fig. (4-g) which also includes the result of Case 9. The experimental conditions of Case 9 were identical to that of Case 0, and in the computations of Case 9, the number of iterations (2) at each time step was the same as for the above three cases.

Case 15 examines the effect of reducing the fuel velocity at the nozzle exit (U_o) on the flame length. The flow rate of Case 15 is about 39% of that of Case 9, and both Cases have the same nozzle diameter. Figure (4-g) shows that $\tilde{x}_{fl}$ for Case 15 is about 2/3 that of Case 9. Furthermore, the value of the dimensional flame length, .0093 m, is in very good agreement with measurements (Ref. 7). At the end of the transient (0-g) mode, however, the predicted flame length is smaller than that for (1-g) condition; this result is in contradiction with experiment. More investigations are required to diagnose the sources of discrepancy in this relatively low Reynolds number Case.

In Case 16, the effect of increasing U_o on the flame length is studied. The flow rate of Case 16 is about 84% larger

than that of Case 9, and both Cases have the same nozzle diameter. Figure (4-g) demonstrates that, as expected, $\tilde{X}_{fL}$ at (1-g) condition is larger for Case 16 than for Case 9. Similar behaviour is also depicted throughout the transient mode.

In Case 18, both the fuel flow rate and the nozzle diameter were respectively 96% and 62% larger than those of Case 9. The transient behaviour of $\tilde{X}_{fL}$ for the two Cases is displayed in Fig (4-g).

Two conclusions can be made from the results of Cases 9, 15, 16, 17 and 18:

a) The predicted values of $\tilde{X}_{fL}$ for the range of flows studied are always less than $\frac{1}{2}$ (see Fig 4-g). This is in agreement with the results of dimensional analysis discussed in detail in Chapter 5.

b) The predicted transient behaviour of $\tilde{X}_{fL}$ at (0-g) for all cases indicates that up to a value of $\tilde{t}$ of about 1.5, $\tilde{X}_{fL}$ decreases as $\tilde{t}$ increases, then $\tilde{X}_{fL}$ starts to increase until it reaches a maximum value. This $\tilde{X}_{fL}$ value is, except for Case 15, larger than its value at (1-g) condition.

The computations for Cases 19 and 20 met some difficulty. In these two cases, the nozzle diameter was respectively about 8.8 and 3.7 times the diameter for the standard Case (0). This, as explained earlier in Chapter 3, required increasing appreciably (10 and 5 times) the lateral width of the integration domain. At the outer cyclindrical boundary of this domain, the radial velocities were calculated from the values of the entrained mass flow rates. These rates were based on the solution of GENMIX program (see Section 2.1). Although

for Cases 0 to 6 and 9 to 14 (nozzle diameter of .102 cm. and domain width 4.5 cm) the solution was not sensitive to the variation of these entrainment rates (see Section 2.1), it is evident from the print-outs of Cases 19 and 20 that the solution becomes sensitive to their values when Y_1 is increased appreciably. This is demonstrated in the predicted distributions of the u-velocity at (1-g) condition of the two Cases. The respective print-outs show large negative u-velocities (recirculation) in the field, associated with a sudden acceleration along the axis and close to the nozzle exit. This is attributed to insufficient entrained fluid at the cylindrical boundary. Detailed investigation of this problem is required.

4.2.8. Examination of the chemical-reaction models

The results obtained from the two chemical-reaction models presented in detail in Section 2.2.4, are discussed here by comparing Cases 0 and 21. The two Cases are identical in both the experimental conditions and the numerical aspects of the solution except for the reaction model employed. Case 0 employs the infinite-rate model while in Case 21, the finite-rate model is used with small value (10.) of the Arrhenius constant to simulate a relatively fast reaction.

The results of both cases are displayed in Fig. (4-h) where the variations of m_{fu} with distance along the nozzle axis are plotted. The figure shows, as expected, that the rate of decay of m_{fu} along the axis is faster in the infinite-rate model than in the finite-rate one.

One can also compare the temperature distributions in the respective print-outs of the two cases. At a given point in the flow, the temperature predicted by the finite-rate model, as one would expect, is less than or equal to that of the infinite rate model.

The transient behaviour of the flame lengths in both cases are also virtually identical (see the print-outs).

4.2.9. The flame extinction study

The search for the reaction-rate constants that produce flame extinction must, of course, be accompanied by a suitable criterion for extinction; one such, is that the maximum temperature in the flow field be less than a specified temperature (e.g. $1000^{\circ}K$). Although we were, in our search, unable to obtain extinction, we can report a definite trend which indicates that a wider range of search for the reaction-rate constants will produce the values suitable for the flame extinction.

It should be pointed out here, that a problem was encountered, during the extinction study, with the convergence of temperature. We can summarize the experience gained in treating this problem by stating that the slower the reaction-rate, the more under-relaxation is required to achieve convergence (see table 3-c for the values of α).

4.2.10. Effect of varying σ_h

The two Cases 0 and 26 are compared to study the effect of σ_h on the solution. In Case 26, σ_h has a value of 0.7 as compared to 0.6 for Case 0; the two cases are otherwise identical.

The transient variation of $\tilde{X}_{fL}$ for both cases are plotted in Fig (4-i). Obviously, the values of the P_T number play an important role in the solution of laminar diffusion-flames.

5 GENERAL DISCUSSION AND CONCLUSIONS

5.1 Comparison of Predicted Results with Expectations Based on Dimensional Analysis

When a laminar steady jet is injected into an atmosphere at rest, the rate of flow of injected-plus-entrained fluid at a section distant x from the nozzle is equal to $8\pi\mu x$, where μ is the fluid viscosity (presumed uniform) and buoyancy effects are absent. [Note that this result, suprising because it is quite independent of the rate of injection, is a consequence of boundary-layer theory; but this theory provides a good approximation in the Reynolds-number range in question here.]

Now 1kg of methane requires about 16kg of air for its complete combustion. We can therefore suppose that, approximately, the flame length will be given by equating $8\pi\mu_\infty x_{fl}$ to 16 times $\rho_o u_o \pi D_o^2/4$; thus:

$$\tilde{x}_{fl} \equiv \left(\frac{x_{fl}}{D_c}\right)\left(\frac{\mu_\infty}{D_c \rho_o u_o}\right) \approx \frac{1}{2} \qquad (5.1\text{-}1)$$

Actually the numerical value of this dimensionless flame length will differ from 1/2 because of:-

(a) the action of buoyancy;

(b) viscosity increases within the flame;

(c) incomplete mixing of the fluid at any section;

(d) elliptic effects;

(e) chemical-kinetic effects.

Factors (a) and (b) tend to diminish the dimensionless

flame length, while factors (c), (d) and, probably, (e) tend to lengthen it. The result is that (5.1-1) can be expected to give good order-of-magnitude estimates.

The flame lengths predicted by the EGOMAC computer program are indeed of the order of magnitude indicated by equation (5.1-1); and they agree with expectations in showing that the dimensionless flame length is smaller, the greater the influence of buoyancy. The dimensionless quantity representing this influence is of course the Froude number which, for present purposes, can be conveniently defined as:

$$F \equiv \frac{u_o^2}{g x_{typical}} \qquad (5.1\text{-}2)$$

Since we might as well define our typical height as the flame length given by the foregoing simple theory, we conclude:

$$F \equiv \frac{2u_o^2}{g D_o}\left(\frac{\mu_\infty}{D_o \rho_o u_o}\right) \qquad (5.1\text{-}3)$$

The transient behaviour can be expected to depend upon a non-dimensional time $\tilde{t}$, for which the normalising quantity is the typical height divided by the injection velocity; thus:

$$\tilde{t} \equiv \frac{2tu_o}{D_o}\left(\frac{\mu_\infty}{D_o \rho_o u_o}\right) \qquad (5.1\text{-}4)$$

We therefore expect that the results for the transient flame length can be represented by way of the following relation between dimensionless groups:

$$\tilde{x}_{fl} = f(F, \tilde{t}) \qquad (5.1\text{-}5)$$

with minor additional effects of Reynolds number, chemical kinetics, and changes in the temperature levels of the injected methane and the surrounding air.

The numerical predictions contained in the present report do confirm this expectation.

5.2 The Influences of Grid and Other Features of the Numerical Solution Procedure

When a phenomenon of this kind is computed numerically, the procedure itself introduces influences which can be expressed thus:

$$\tilde{X}_{fl} = f\left(F, \tilde{t}, \delta\tilde{t}, \frac{r_{max}}{D_o}, \frac{x_{max}}{D_o}, \frac{\mu_\infty}{\rho_o u_o D_o}, N_r, N_x, N_{it}, \cdots\right) \qquad (5.2\text{-}1)$$

This expression indicates that:-

- the dimensionless time step, $\delta\tilde{t}$, influences the result;
- the size of the domain of integration, represented by r_{max}/D_o and $x_{max}/x_{typical}$, has some effects;
- the numbers of grid lines in each of the two co-ordinate directions, as well as departures from uniformity of spacing, also affect the predicted flame length;
- the number of iterations per time step, and other details of the procedure such as the order in which the equations are solved at each time step, all have their influence on the computed results.

Of course, with a satisfactory prediction procedure, $\delta\tilde{t}$, N_r, N_x etc are all given such values as render their influence small; but what those values are can be established only by systematic exploration.

The investigation reported in the present paper represents only an initial phase of the exploration.

However, it is evident that sufficient information has been accumulated to enable the next phase to be planned successfully.

5.3 The Influences of the Properties Presumed

If the grid were fine enough and the time step extremely small, we can be sure that the solution of the finite-difference equations would be identical with that of the differential equations; whether it would agree with experimental data is, however, an entirely different matter.

In the EGOMAC computer program as currently constituted, the formulations of the thermodynamic, transport and chemical-kinetic properties are simple ones, as is entirely appropriate to an exploratory investigation. Thus, the heat-conduction and material-diffusion processes are represented by constant Prandtl and Schmidt numbers; and the complexities of the real chemical-kinetic processes are all hidden within the two free constants of an Arrhenius reaction-rate expression.

Because of this, and of the fact that there are many more parameters to vary even within this limited conceptual framework than could be investigated during the present explorations, it is not surprising that there are disagreements between the predictions made by the EGOMAC computer program and the available experimental data. Indeed, it is very gratifying that the agreement is so good, both qualitatively and quantitatively.

What is now needed is a two-part investigation in which, first, the disposable constants of the present model are varied so as to optimise the agreement over the whole range of conditions, and, secondly, even better

agreement is sought through the introduction of refinements to the model. These refinements should include more realistic formulations for thermodynamic and transport properties and for reaction kinetics.

5.4 The Influences of the Boundary Conditions

Problems of this "elliptic" kind require specification of boundary conditions at all boundaries of the domain; yet these are rarely known.

In the EGOMAC computations, a fixed-rate-of-entrainment boundary condition has been imposed, the entrainment rate being chosen as that which a simplified analysis dictates. Although there is no reason to suppose that the nature of this boundary condition significantly affects the computation in the central physically-interesting region, a further investigation is needed before the point can be established with certainty.

5.5 Computational Economy

Because of the low limit on available funds for this project, no program development was done. The EGOMAC therefore does not contain all the devices for economising computer time and storage which are available in more recent CHAM codes, and in others under development.

It should therefore be mentioned that the EGOMAC code is rather expensive to run. For a given numerical accuracy, improvements could be incorporated which would reduce its running costs to below 50% of the present level.

5.6 Recommendations for Further Work

This investigation has firmly established that computations of the kind performed by EGOMAC are potentially capable of correctly predicting the transient buoyant laminar diffusion-flame process that formed the centrepiece of the project; and of course it confirms belief that many other flame and flow processes can be predicted by extensions of the method. To this extent, the investigation can be counted as successful.

However, the success requires to be exploited; and, of the various directions in which future work can go, the following appear to be especially fruitful:-

(a) Improvements of computational economy

Because it is now desirable to exercise the EGOMAC code extensively, the cost of doing so should be reduced by measures directed to improving computational efficiency. There are many of these available; and they will become especially valuable when finer grids are employed in the interests of improved accuracy.

(b) Optimisation of physical inputs

If a closer fit is required between the predictions and measurements for the transient methane-air flame, it will be necessary to optimise the various inputs. For example, the assumption of a single uniform Schmidt number for diffusion of all components is certainly not correct; it could be replaced by assuming individual Schmidt numbers for each component; and of course the Stefan-Maxwell equations could be introduced as a more realistic alternative.

If extinction phenomena are to be realistically

predicted over a range of experimental conditions, there is no doubt that an appreciably more complex chemical-kinetic model will be needed than the present one. Although it would have been possible, had more funds and time been available, to extend the search for optimum constants for the Arrhenius equation, this would be hard to justify until the physical properties have been optimised.

(c) Employment of simpler computational schemes

It is possible, with hindsight, to recognize that the EGOMAC computer code is too complex and expensive for some of the tasks of interest to the sponsor. Thus, since the parabolic equations represent a good approximation to the steady-state situation, and since such equations can be solved (eg by way of GENMIX, Ref 8) more expeditiously than the elliptic ones, it would make sense to optimise the transport-property inputs by an extensive investigation of steady-state flames.

(d) Application to different systems

Now that EGOMAC has shown its potential for the methane-air flame, it can evidently be employed with some confidence for other flame systems also. Thus:

- The reactants can be changed.
- The boundary conditions may be altered.
- Gravity may vary with time in accordance with a different program from the all-or-nothing prescription of the present example.
- Turbulence may be introduced.
- NOX reactions may be studied.
- Etc.

Further, it should not be forgotten that EGOMAC is just one member of a family of computer codes, which includes

those capable of handling three-dimensional unsteady flames.

5.7 Summary of Conclusions

(a) The EGOMAC computer code has been shown to be capable of meeting the sponsor's requirements.

(b) Many more computer runs have been made than were required by the client; and their results are reported and summarised in this document.

(c) It has been shown that the experimental behaviour can be reproduced with fair accuracy, provided that the time step is sufficiently short. Iteration at each time step also improves accuracy.

(d) Further improvement of agreement between predictions and experiment can also be achieved by modification of physical-property data within reasonable limits.

(e) Exploitation of the success requires further work in respect of:-

- Improvements to computational efficiency.
- Optimisation of physical inputs.
- Conduct of supporting investigations by way of simpler computer codes.
- Extension to different and more complex flame systems.

6. References

1. Hottel, H.C. and Hawthorne, W. "Diffusion in Laminar Flame Jets", Third Symposium on Combustion, Flame and Explosion Phenomena, Williams and Wilkins Co., 1949.

2. Wohl, K., Gazley, C. and Kapp, N. "Diffusion Flames", Third Symposium on Combustion, Flame, and Explosion Phenomena, Williams and Wilkins Company, 1949.

3. Burke, S.P. and Schumann, T.E., "Diffusion Flames", Industrial and Engineering Chemistry, v, 20, No. 10, p.p. 998-1004, October 1928.

4. Goldburg, A., Cheng Sin-I, "A Review of the Fluid Dynamic Problem Posed by the Laminar Jet Diffusion Flame", Combustion and Flame, v. 9, No. 3, September 1965, p.p. 259-272.

5. Cochran, T.H. and Masica, W.J., "Effects of Gravity on Laminar Gas Jet Diffusion Flames," NASA TN D-5872., June 1970.

6. Cochran, T.H. and Masica, W.J. "An Investigation of Gravity Effects on Laminar Gas Jet Diffusion Flames," NASA TM X-52757, August 1970.

7. Edelman, R.B., Fortune, O. and Weilerstein, O. "Analytical Study of Gravity Effects on Laminar Diffusion Flames". NASA CR-120921 February 1972.

8. Patankar, S.V. and Spalding, D.B. "Heat and Mass Transfer in Boundary Layers", 2nd Edition Intertext Books, London 1970.

9. Patankar, S.V. and Spalding, D.B. "A calculation Procedure for Heat, Mass and Momentum Transfer in Three-dimensional parabolic flows", Int. J. Heat Mass Transfer, 15, p.p. 1787-1806, 1972.

10. Spalding, D.B. "A Novel finite difference formulation for differential expressions involving both first and second derivatives", Int. J. Num. Meth. in Engineering, 4, p.p. 551-559, 1972.

7. NOMENCLATURE

Symbol	Meaning
a	radiation absorption coefficient
a_x, a_{y+}, a_{y-}	cell-face areas
A	constant in the Arrhenius reaction-rate expression
A_j, B_j	coefficients in Sutherland law for viscosity of species j
A_p, A_{x+}, A_{x-}, A_{y-}	coefficients in the finite-difference equations
C_j,n	coefficients in the expression for enthalpy of species j
D	nozzle diameter
D^u, D^v	pressure-term coefficients in the finite-difference equations for u and v
E	black body emissive power
E^u, E^v	coefficients in the correction formulae for u and v
f	mixture fraction
g	gravitational acceleration
h	enthalpy
H	lower value of the heat of formation of methane
i	stoichiometric ratio
I, J	radiative heat fluxes in the positive and negative r direction
K, L	radiative heat fluxes in the positive and negative x direction
m	mass fraction
M	molecular weight

M_p	mass source at grid node P
p	static pressure
r	radial distance
R	flame radius
R_x, R_r	radiation flux quantities
$\mathcal{R}$	universal gas constant
s	scattering coefficient for radiation
	source term
S_u, S_p	coefficients in the linearised source term
t	time
T	temperature
u	axial velocity
v	radial velocity
x	axial distance
x_{fl}	flame length
y	radial distance
Z	constant in the Arrhenius reaction rate expression
α	under-relaxation factor
Γ	diffusion coefficient
$\delta x, \delta y$	cell dimensions
μ	laminar viscosity
ρ	density
σ_ϕ	Prandtl/Schmidt number
σ	Stefan - Boltzmann constant
ϕ	general dependent variable
$\Psi(x)$	mass flow rate of entrained fluid along cylindrical boundary up to x

Subscript	Pertaining to
CO_2	carbon dioxide
fu	fuel (methane)
H_2O	water vapor
j	species j
N_2	nitrogen
ox	oxygen
P	grid node P
st	stoichiometric conditions
X+, X-, Y+, Y-	neighbourning grid nodes
ϕ	variable ϕ
O	conditions at the nozzle
∞	ambient conditions

Superscripts	Pertaining to
n	conditions at the present time step
o	conditions at the previous time step
u, v	velocities u and v
'	corrections to estimated pressures and velocities
*	estimated quantities
—	mean values within the flame
~	dimensionless quantity

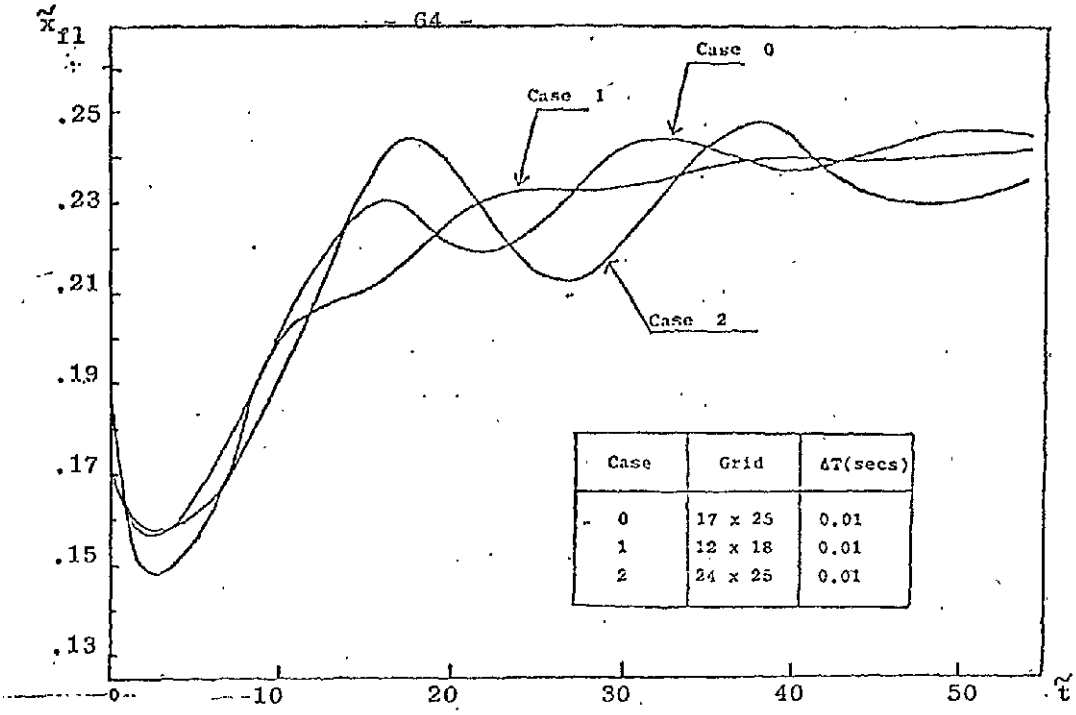

Fig. 4-a : The Effect of the Grid Refinement on the Transient Behaviour of the Flame Length

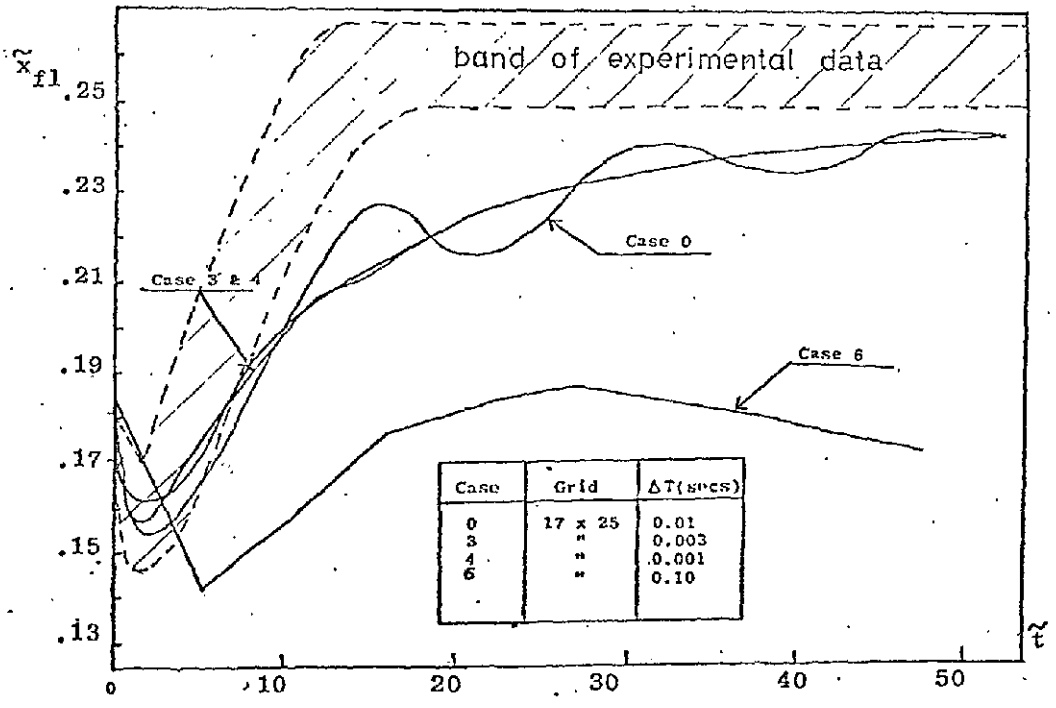

Fig 4-b: The Effect of the Time Step on the Transient Behaviour of the Flame Length

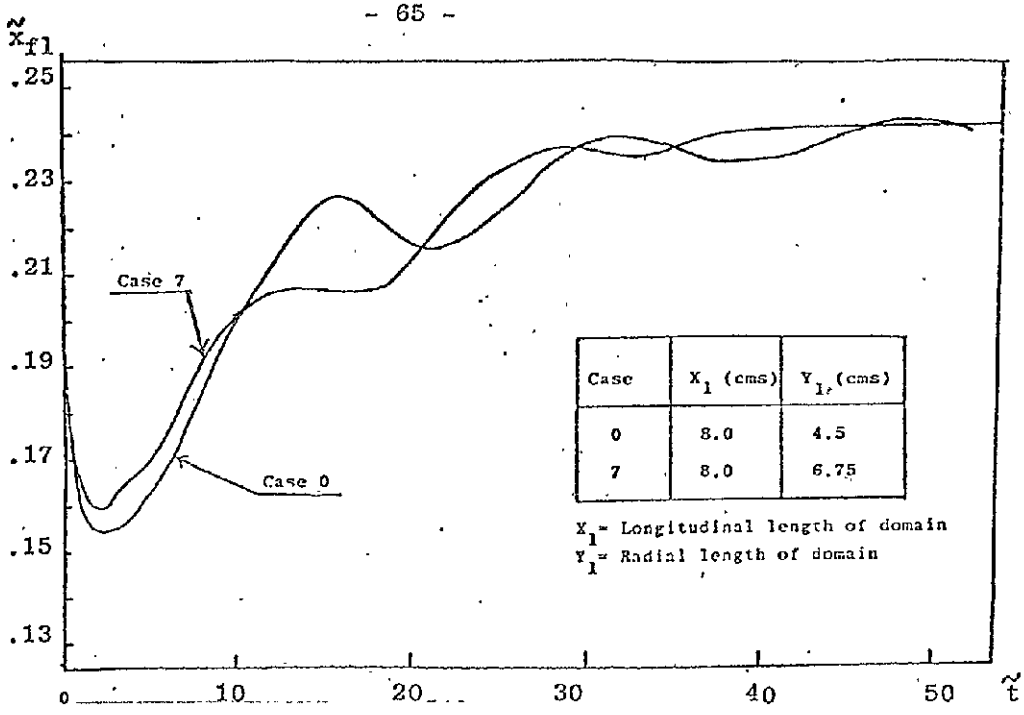

Fig 4-c: The Effect of Increasing the Radial Width of the Integration Domain on the Transient Behaviour of the Flame Length

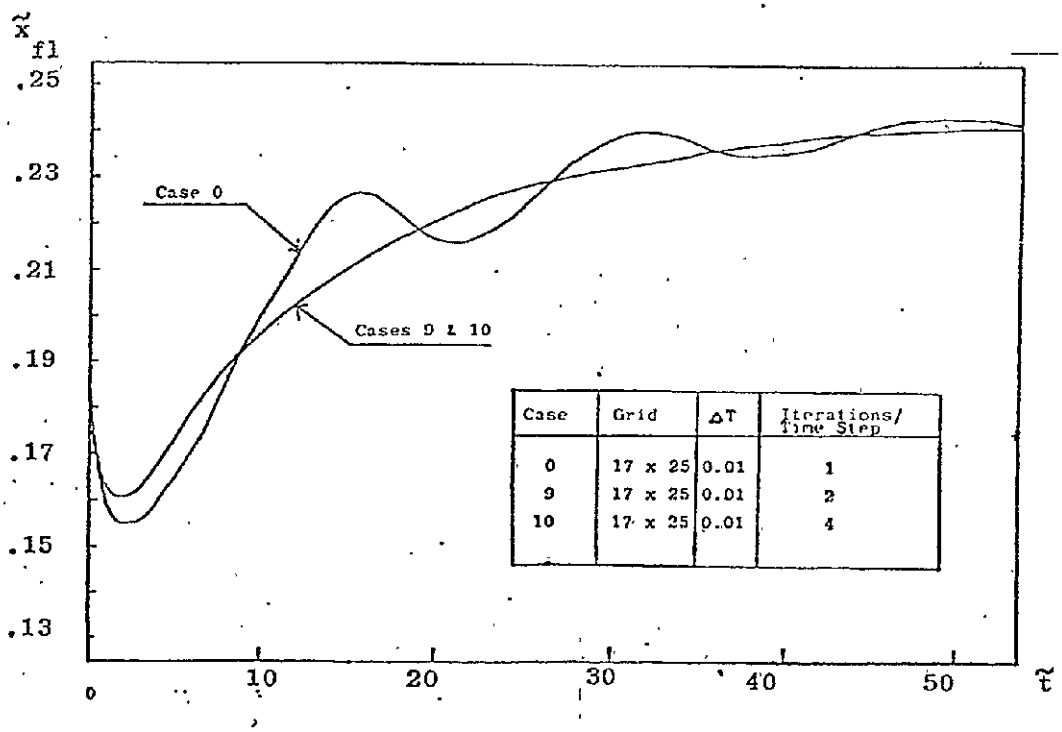

Fig 4-d : The Effect of Increasing the Number of Iterations at each Time Step on the Transient Behaviour of the Flame Length

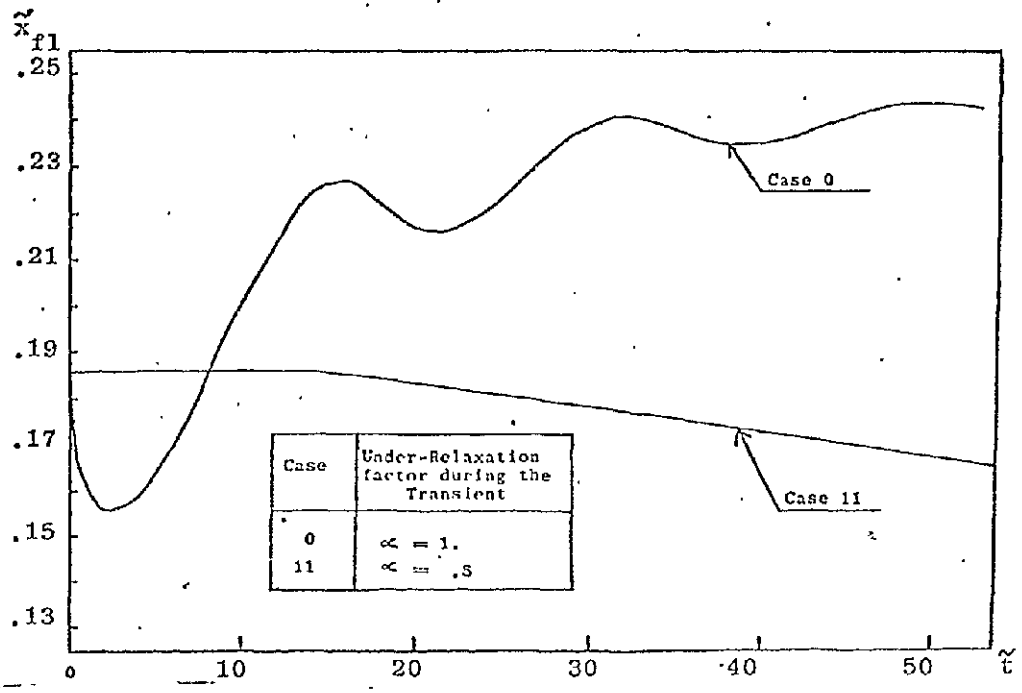

Fig 4-e: The Effect of Under-Relaxing the Dependant Variables on the Transient Behaviour of the Flame Length

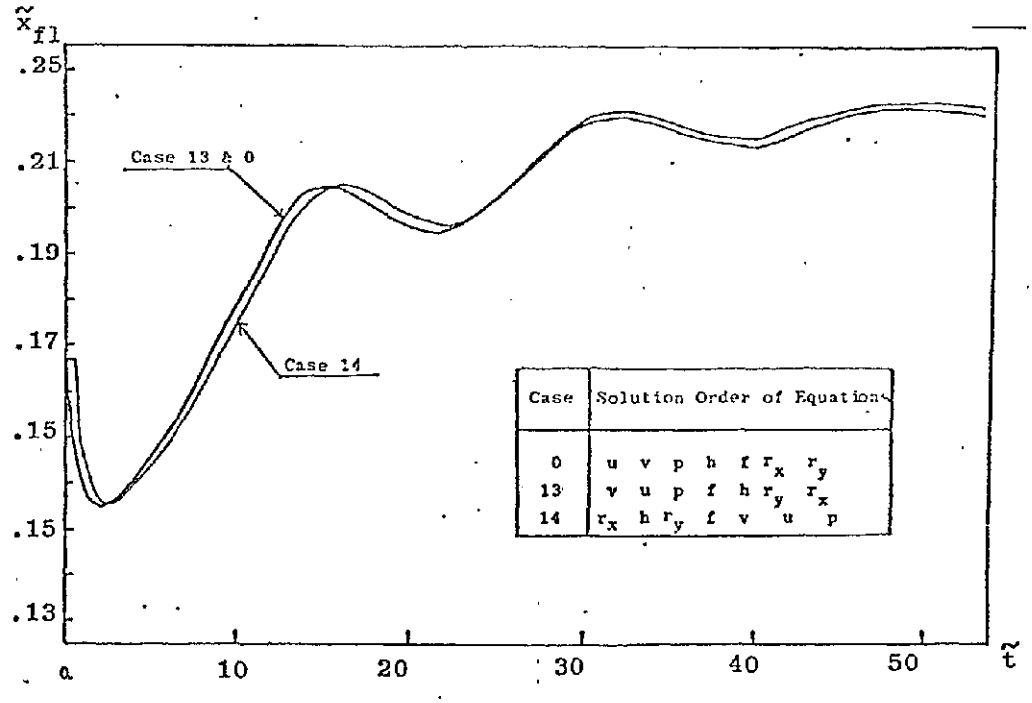

Fig 4-f: The Effect of changing the Solution Order of the Differential Equations on the Transient Behaviour of the Flame Length

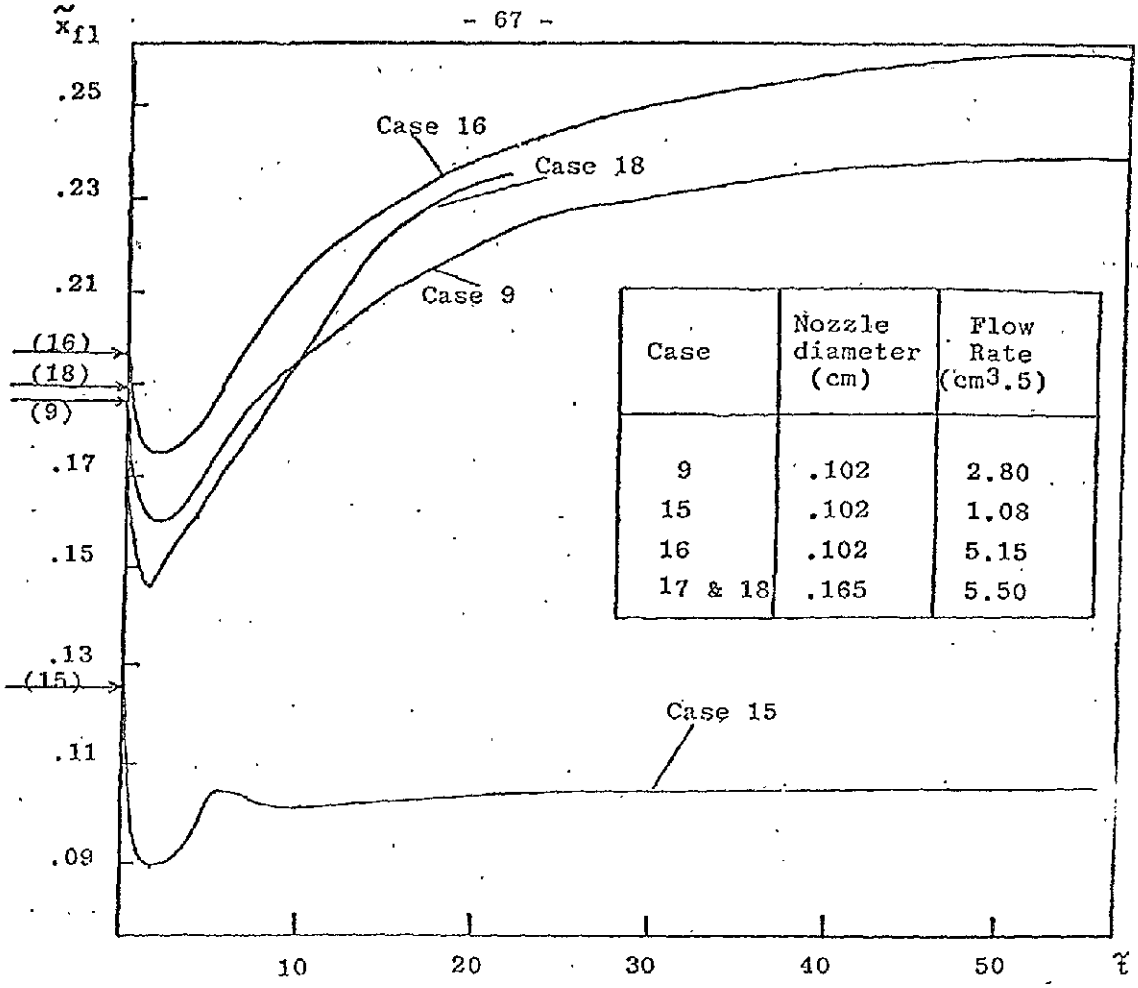

Case	Nozzle diameter (cm)	Flow Rate ($cm^3.5$)
9	.102	2.80
15	.102	1.08
16	.102	5.15
17 & 18	.165	5.50

Fig 4-g: The effect of Nozzle Diameter and Volumetric Flow Rate

* Arrows indicate $\tilde{x}_{f1}$ values at (1-g) condition.

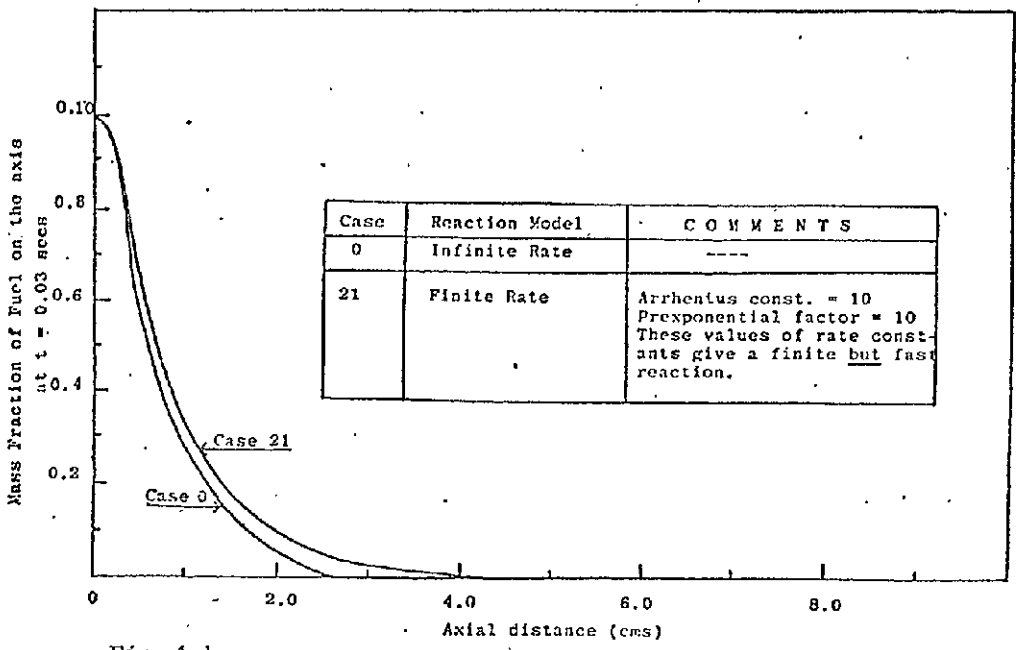

Case	Reaction Model	COMMENTS
0	Infinite Rate	----
21	Finite Rate	Arrhenius const. = 10 Prexponential factor = 10 These values of rate constants give a finite but fast reaction.

Fig 4-h : A comparison between a Fast Finite-Rate Reaction and a Infinite-Rate Reaction for the Flow Condition of Case O

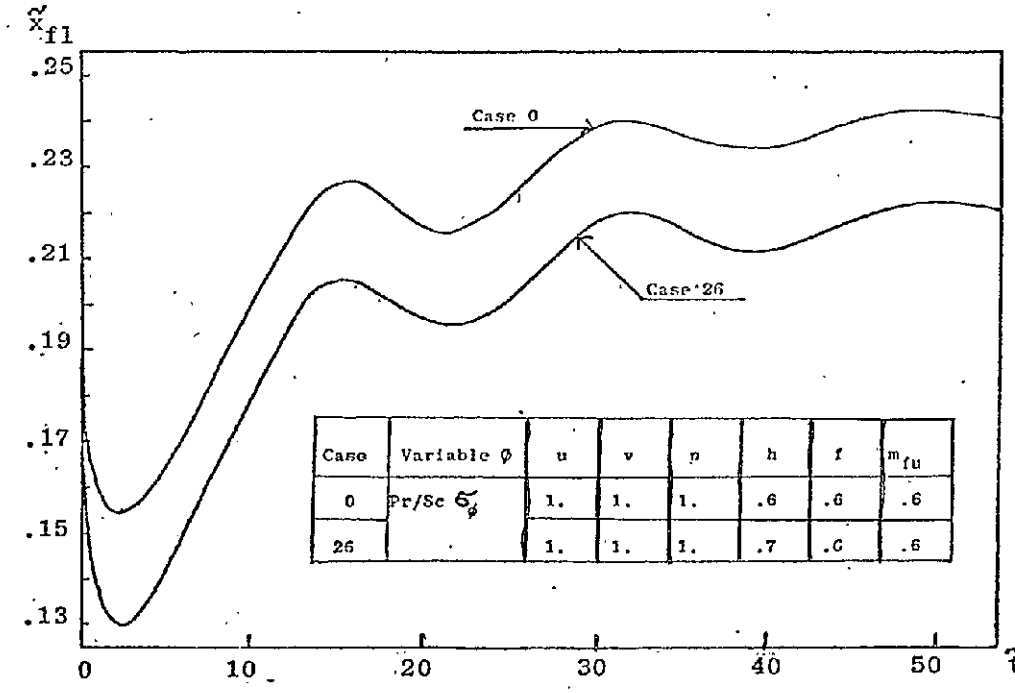

Case	Variable ϕ	u	v	p	h	f	m_{fu}
0	Pr/Sc σ_ϕ	1.	1.	1.	.6	.6	.6
26		1.	1.	1.	.7	.6	.6

Fig 4-i : Effect of Increasing the Enthalpy Prandtl number on the Transient Behaviour of the Flame Length

A P P E N D I X

THE PRINT-OUT FORMAT

This appendix is intended as an aid to the reader of the computer output which accompanies this report. At each time step or after each iteration, several quantities are printed, and these are now to be individually discussed.

TIME - The period during which the flame has been subjected to zero-gravity conditions. In some of the cases,e.g. Case 0, iteration is at first employed to obtain a (1-g) converged steady-state solution and for this situation TIME = 0. In other cases a converged steady-state solution is stored (as a permanent file on computer disc storage), and is used to provide initial conditions.

LFLAME-The flame length along the axis of symmetry. The flame envelope, or surface, is defined to be the locus of points, in the flow field, for which the mixture fraction obtains the stoichoimetric value. The flame length is determined by interpolation between appropriate grid nodes at the axis of symmetry.

WFLAME-The maximum width of the flame, This quantity is determined by finding the width of the flame envelope along all the grid lines parallel to the y-axis. For any given grid line the envelope width is obtained by interpolation between the appropriate grid nodes. The maximum of these envelope widths is set to WFLAME.

U AT LF-The axial velocity at the tip of the flame. This quantity is also determined by interpolation.

The mixture fraction is printed out at 8 locations along the axis. These locations are taken as fractions and multiples of the flame length (e.g. at $x = 0.5 \times LF$)

The remaining quantity which is printed out at each time step is the temperature at the nodal points along the axis and along the grid line which corresponds to the maximum width of the flame envelope.

Finally more comprehensive print outs are given at the following instants.

t = 0.0, 0.03, 0.1, 0.3, 0.5, 0.7, 1.0 secs.

The variables printed out are:-
u, v, m_{N_2}, h, m_{fu}, m_{ox}, T, R_x, R_y, pp, each at approximately 100 points in the flow field.

ORIGINAL PAGE IS
OF POOR QUALITY